

Quantitative optical coherence tomography of fluid-filled oral mucosal lesions

O. K. Adegun · P. H. Tomlins · E. Hagi-Pavli ·
D. L. Bader · Farida Fortune

Received: 22 February 2012 / Accepted: 7 September 2012 / Published online: 21 September 2012
© Springer-Verlag London Ltd 2012

Abstract The decision of selecting the most representative site for the biopsy of fluid-filled lesions can be difficult. This may be attributed to the poor delineation of the correct lesional site by clinical observation alone. In this study, optical coherence tomography is used to quantify the contrast between solid- and fluid-filled lesions by measuring the light intensity change at the tissue–fluid interface (intensity drop). This parameter was measured from sequential axial scans ($n \approx 10^6$ per sample) of 3D optical coherence tomography (OCT) datasets from control tissues ($n=14$) and fluid-filled lesions ($n=7$) and displayed as a 2D-scaled intensity drop (SID) image. The results of the SID image allowed for discrimination, characterisation and extent of a fluid filled region. The differentiation of normal and fluid-filled areas using individual SID values yielded both a sensitivity and specificity of approximately 80 %. OCT complemented by SID analysis provides a potential in vivo clinical tool that would enable non-invasive objective visualisation of the oral mucosa.

Keywords Imaging · Biophotonics · Oral pathology · Oral medicine · Oral diagnosis · Optical coherence tomography · Morphometric

Introduction

Oral fluid-filled lesions vary in number and size, with the relative diameter ranging from small vesicles (<0.5 cm) to

large bullae (>0.5 cm). The aetiology of these lesions also varies and may be due to a number of clinical conditions including infection, inflammation, trauma, allergic reaction and other pathological processes. Despite this plethora of aetiological factors, a common feature to all fluid-filled oral mucosal lesions is the accumulation of either mucinous, inflammatory exudate or blood between the epithelial and/or the superficial lamina propria layers of the oral mucous membrane. The variety of causes makes it difficult to establish an accurate diagnosis based on clinical symptoms and presentation, hence the need in most cases to perform a biopsy and histological examination. This is especially difficult when there are multiple independent lesions presenting with similar clinical features. Indeed, taking a biopsy from fluid-filled lesions is fraught with difficulty when deciding upon location and lesion site to biopsy. Even when a diagnosis has been established, some fluid-filled lesions require regular follow-up to monitor treatment. It would therefore be beneficial to introduce a non-invasive imaging modality to assess the micro-morphological features identified in histopathology.

One potential technique is optical coherence tomography (OCT) [1], which uses near infra-red light to non-invasively produce cross-sectional images of tissue morphology analogous to ultrasound B-scans [2, 3]. This technique is capable of imaging tissue depths of up to 1–2 mm and thus considered suitable for the superficial location associated with many oral mucosal lesions [4]. Recent studies have demonstrated the feasibility of using OCT to image oral lesions including epithelial dysplasia [5], vascular malformations [6] and submucous fibrosis [7]. Despite the technology, there is very little evidence of the relationship between OCT contrast and specific pathological states [5, 8–11]. Furthermore, the challenge of discerning tissue morphology in OCT necessitates a new approach for presentation of clinical information [10–12]. An area of growing interest for OCT research is that of quantitative

O. K. Adegun · P. H. Tomlins · E. Hagi-Pavli · F. Fortune (✉)
Centre for Clinical and Diagnostic Oral Sciences, Institute of
Dentistry, Barts and The London School of Medicine and Dentistry,
4 Newark Street, Whitechapel,
E1 2AT London, UK
e-mail: f.fortune@qmul.ac.uk

D. L. Bader
Faculty of Health Sciences, University of Southampton,
Southampton, UK

parameterisation. Recent research has focussed upon measuring the tissue-scattering coefficient to differentiate between healthy and diseased states. This approach has been applied to tissue examination in various medical specialties, including assessment of potentially malignant renal masses [13, 14] and spatial attenuation mapping of oral pre-cancer [11], atherosclerotic tissue [15] and human axillary lymph nodes [16]. The present paper introduces a new mode of visualisation for OCT called scaled intensity drop (SID) imaging. SID is designed to discriminate between solid- and fluid-filled oral mucosal tissues and would be appropriate for early detection, accurate biopsy sampling and monitoring of fluid-filled lesions.

Materials and methods

Biological probes

To test the ability of SID to discriminate between solid- and fluid-filled regions of tissue, human oral mucosa biopsy specimens were examined. For this study, the control group of solid tissue comprised histologically normal tissue ($n=2$) and fibroepithelial polyps ($n=12$). The group of specimens containing fluid-filled areas was identified histologically as mucoceles ($n=7$). Details of each biopsy specimen are given in Table 1. All biopsies were obtained as part of routine clinical care from patients attending the Oral Medicine Clinic of Barts and The London Hospital following approval from the local ethical review committee and informed patient consent. Biopsy samples included in the study were those that had a provisional clinical diagnosis of fibroepithelial polyp or oral mucocele. Samples were excluded if there was a mismatch between the provisional diagnosis and histopathology, the gold standard. However, following the final histopathology reports, none of measured samples were excluded.

OCT system

An EX-1301 OCT microscope (Michelson Diagnostics Limited, Kent, UK) was used in this study. The system represents a swept-source, Fourier Domain OCT system incorporating a Santec-HSL-2000 light source with a peak wavelength of $1,305 \pm 15$ nm as specified by the manufacturer. The axial and lateral resolutions in air were approximately 11 and 8 μm , respectively. The source spectrum and system resolution have been characterised in previous work [17] and found to agree with the above-quoted specifications.

OCT Calibration

For comparison of measurements used in this study, the OCT instrument dynamic range and its depth dependency

Table 1 Mean and standard deviation SID values for all patients

Sample	Site	SID dB/mm	
		Mean	Standard deviation
N1	Lower lip	5.0	1.6
N2	Palate	5.3	1.7
FEP1	Buccal mucosa	5.6	1.2
FEP2	Gingiva	5.8	1.7
FEP3	Buccal mucosa	3.5	1.5
FEP4	Dorsum of tongue	6.2	1.7
FEP5	Gingiva	5.5	1.3
FEP6	Lateral border of tongue	7.0	1.5
FEP7	Dorsum of tongue	6.1	1.4
FEP8	Dorsum of tongue	5.1	1.6
FEP9	Dorsum of tongue	7.2	1.8
FEP10	Lower lip	7.1	2.8
FEP11	Buccal mucosa	5.1	1.8
FEP12	Gingiva	5.4	1.9
MC1	Lower lip	8.3	2.4
MC2	Lower lip	9.2	2.7
MC3	Lower lip	10.3	3.0
MC4	Upper lip	13.8	3.6
MC5	Buccal mucosa	17.5	8.7
MC6	Buccal mucosa	14.4	5.6
MC7	Lower lip	11.3	4.4

N Normal tissue, *FEP* Fibroepithelial Polyp, *MC* Mucocele cyst

are critical parameters. Prior to each measurement, the OCT instrument was characterised by imaging a known scattering phantom. The optical properties of this phantom have previously been described [18]. The phantom provides a simple way to determine sensitivity variations throughout the imaging plane. For this work, a phantom having a scattering coefficient of $\mu_s=0.6 \text{ mm}^{-1}$ was used. According to previous research [19], such a phantom will exhibit an OCT signal attenuation slope that is dominated by single scattering over the considered OCT depth range of 4 mm. Consequently, this facilitates calibration of intensity variations due to a focussed sample beam and non-uniform sensitivity. For example, under single scattering conditions and negligible absorption, the OCT signal (I) is expected to follow an exponential decay as a function of depth (z) governed by the equation

$$I(z) = A(z) \exp(-\mu_s z). \quad (1)$$

In Eq. 1, $A(z)$ is an amplitude function that perturbs the expected OCT signal and can include factors such as variations in system sensitivity and detection efficiency throughout the beam waist. Since OCT data are generally considered in

the logarithmic domain, $\log(I(z))$ is the sum of a decay function and amplitude function. Thus, given that the decay function for our phantom is previously known, the logarithmic amplitude function is determined by subtracting the decay function from the measured data. The resulting amplitude correction is subtracted from all subsequent OCT measurements.

OCT imaging procedure

Each biopsy sample was orientated on the stage of the microscope such that the mucosal surface was approximately perpendicular to the OCT incident beam. Excess liquid was removed from the tissue surface using a cotton swab. A precisely fixed incident angle was not maintained throughout imaging due to the contoured surface topography of each sample. The sample position was adjusted such that its highest point was just below the top of the OCT B-scan field of view. The optical focus was approximately uniform throughout the epithelial depth of the sample, owing to the unique multi-foci configuration of the particular OCT device used. This has previously been independently measured [17]. Volumetric OCT images were collected by acquiring sequential cross-sectional (B-scan) images at 5 μm intervals along the biopsy length with the aid of a motorised stage under computer control. The samples were then processed, paraffin embedded, sectioned at 5 μm interval and stained with haematoxylin and eosin. Structurally similar features identified in OCT images were visually compared with corresponding histology. To aid in this comparison, average depth profiles were also visually compared for both greyscale histology images and corresponding OCT as described previously [11].

Scaled intensity drop analysis procedure

The OCT image data were specifically processed to detect the large intensity drop that was typically observed to occur at the boundary between solid tissue and regions of fluid compared with normal controls. This is demonstrated visually in Fig. 1. It is important to note that the resulting SID parameter is not exactly equivalent to the traditional attenuation coefficient. Instead, it is best described as a quasi-attenuation measurement utilising the same units. In order to identify the characteristic intensity drop, a simple algorithm was developed as described below.

For each A-scan, the logarithmic intensity was summed along its depth as indicated by the cumulative intensity curve in Fig. 1. Two points along the A-scan were then selected. The first point was chosen to coincide with the 5 % level of the cumulative intensity curve and the second with the 90 % level. These are depicted in Fig. 1 by the dashed and dotted lines, respectively. The depth difference between the two lines has been termed the attenuation depth [11] and the change in intensity over this range is called the intensity drop. The SID

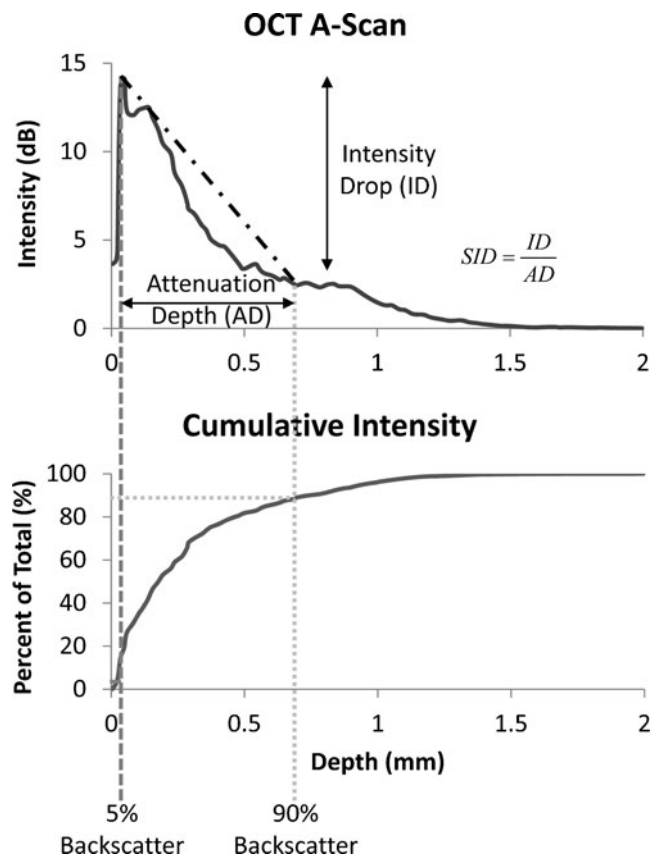


Fig. 1 The scaled intensity drop (*SID*) is a quasi-measure of attenuation determined as the ratio of intensity drop (*ID*) to attenuation depth (*AD*). The attenuation depth is an estimate of the optical penetration distance before 85 % of the OCT signal is attenuated

is calculated as the ratio of intensity drop to attenuation depth. Practically, noise was rejected from the cumulative sum by using an intensity filter that rejected intensity values within 2 standard deviations of the mean background noise. Furthermore, the effect of speckle noise is effectively averaged by the cumulative summation. The SID for all A-scans within a selected three-dimensional OCT volume was used to assess the variation in this parameter. Analysis software was written in-house using MatLab mathematical programming language (MathWorks Corp., CA, USA), thereby enabling large quantities of data to be processed automatically.

SID values ($n \approx 10^6$ per sample) were obtained from a normal control sample group comprising histologically normal tissue ($n=2$) and fibroepithelial polyps ($n=12$). Values of fluid-filled tissue areas were identified in biopsied mucocoeles ($n=7$). In each dataset, an area of affected tissue was selected for analysis, guided by the OCT B-scan images.

Data analysis

The purpose of our analysis was to determine whether the SID parameter is sensitive to the presence of fluidic lesions.

To achieve this, a control group of solid oral mucosal (SOM) samples ($n=14$) was compared with fluid-filled tissue specimens ($n=7$). Three-dimensional OCT datasets were acquired from each sample, from which approximately $n=10^6$ SID measurements were obtained. SID measurements for the SOM group were obtained for all A-scans within the measured volume. However, the specimens containing fluidic regions inevitably also comprised regions of SOM. Consequently, from these samples, fluidic regions were identified by visually correlating structurally similar features in OCT B-scans with histology. The extent of the fluid-filled region was estimated in the 3D OCT image datasets based upon their characteristic features, i.e. low signal intensity below the epithelium. SID values were calculated for each A-scan within the selected volume and compared to values for SOMs. This bootstrapping technique was necessary because a full three-dimensional set of pathology slides was not available. Intra-group comparison of the SID values for each of the fluid-filled and control groups was accomplished using a two-tailed t test, assuming equal variance within samples of the same classification. For inter-group comparison, un-equal variance was assumed.

Results

Histologically, normal oral mucosal tissue is characterised by a distinct layered structure, comprising the overlying epithelium and underlying lamina propria, as shown in Fig. 2a. The interface between both layers is demarcated by the basement membrane. In contrast, the mucocele histology (Fig. 2b) was characterised by a homogenous region

of fluid-containing areas of granulation tissue beneath the epithelium. The OCT images in Fig. 2c, d were carefully matched to their corresponding histology (Fig. 2a, b) for qualitative comparison with the gold standard. In comparison to Fig. 2c, the absence of connective tissue in the fluid-filled area was readily identifiable in the corresponding OCT (Fig. 2d) by the low signal intensity. This is reflected in the averaged depth profile (Fig. 2d) whereby the transition from the epithelium to the fluid-filled area manifested as a sharp discontinuity in the image intensity compared with normal tissue (Fig. 2d).

In this study, volumetric OCT datasets from normal (N), fibroepithelial polyp (FEP) and mucocele (MC) biopsy samples were subjected to SID analysis. The site of biopsy and resulting mean and standard deviation SID value for each sample are shown in Table 1.

Measured SID values from normal and FEP samples were found to be similar in terms of their statistical distributions ($p=0.39$). Accordingly, for subsequent analysis, these two sample groups were categorised as SOM samples (controls). The pooled SOM SID measurements were compared to the SID measurements from the MC group and the difference in the means was found to be statistically significant ($p\leq 0.05$). However, the associated SID value distributions from both the SOM ($n\approx 14\times 10^6$) and fluid-filled MC ($n\approx 7\times 10^6$) sample groups revealed an area of overlap (Fig. 3a) leading to a degree of classification uncertainty for individual SID measurements. This was quantified in terms of sensitivity and specificity for a continuous range of SID threshold values, resulting in the smooth curve in Fig. 3b. Such analysis was made possible by well-defined SID distributions (Fig. 3a) that comprised all measurements.

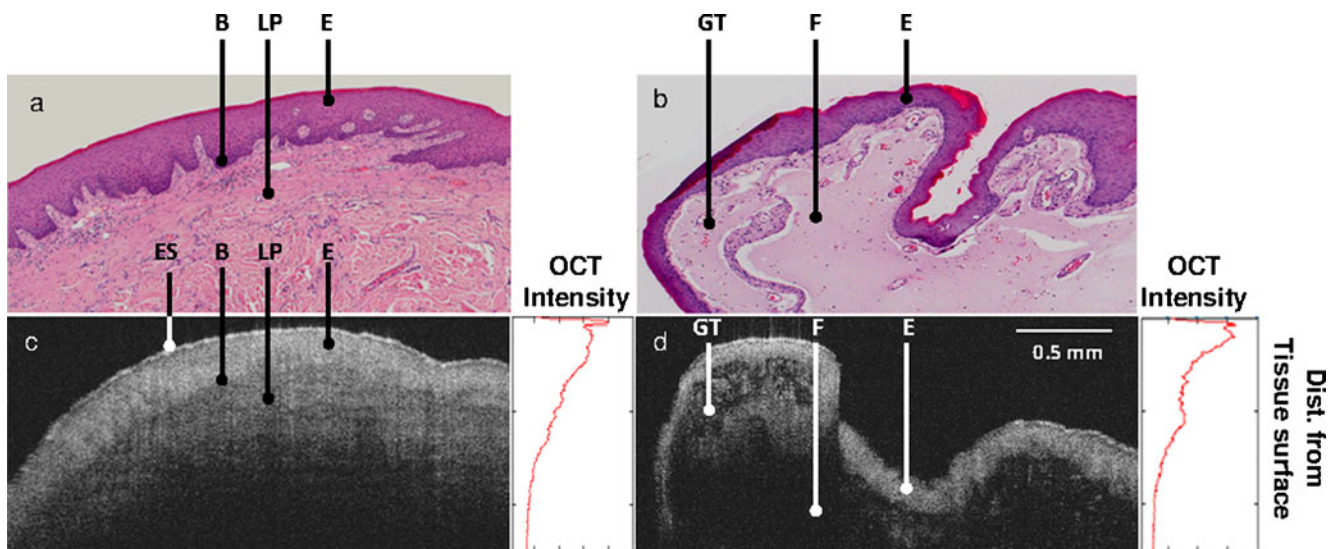


Fig. 2 Histology images of clinically normal buccal mucosa (a) and mucocele of the lower lip (b). The corresponding OCT images are shown in c and d, respectively. The insets represent the averaged depth

intensity profiles for each image. *ES* entrance signal, *E* epithelium, *LP* lamina propria, *GT* granulation tissue, *E* epithelium, *F* fluid

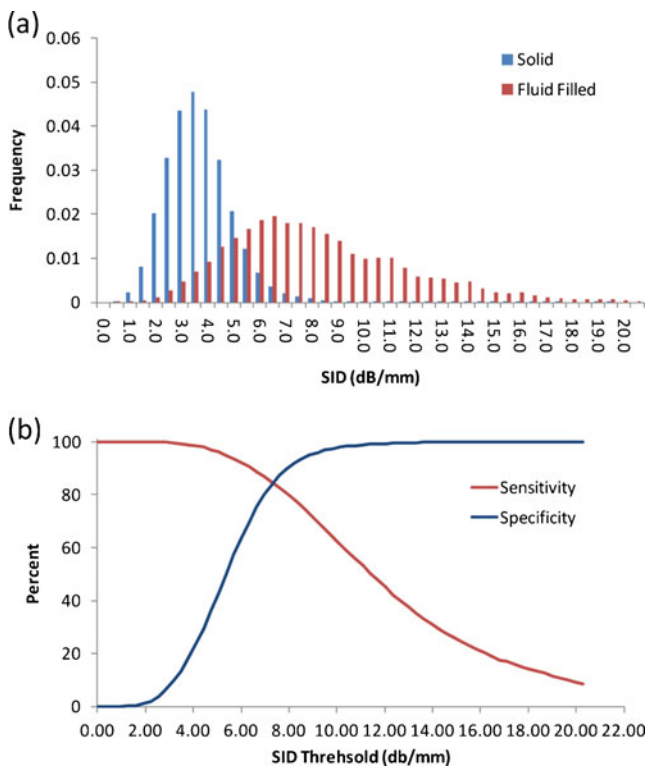


Fig. 3 **a** Normalised histograms representing all SID values from the normal controls ($n=14$) and mucoceles ($n=7$). **b** Sensitivity and specificity of SID values for classification between normal and fluid-filled tissue. Values falling below the SID threshold are considered normal and those above classified as fluid filled

SID values below the threshold were considered normal and those above were classified as fluid filled. A threshold value of 7.0 dB/mm was evident, for which both sensitivity and specificity yielded values of approximately 80 %.

Unlike histology (Fig. 4a–d), individual SID values are unable to provide information regarding spatial distribution or extent of lesion. For ease of clinical interpretation, it is valuable to present SID values as a 2D, false colour en face image. As an example, Fig. 4e–h shows greyscale light intensity images of two SOM samples (N1 and FEP8) and two fluid-filled lesions (MC2 and MC3). Below these (Fig. 4i–l) are the corresponding SID images, within the range of 0–20 dB/mm, calculated from the 3D OCT dataset of each sample.

It can be seen that the SOM samples show a relatively homogeneous distribution of SID values, with 95 % in the range 2.0–8.8 dB/mm. By contrast, SID images of the mucoceles show localised areas of high SID in the range 3.7–13.2 dB/mm. Notably, in Fig. 4k (MC2), the fluid-filled region was highlighted towards the top left of the sample. By contrast, Fig. 4l showed extensive areas of fluid accumulation interspersed with discrete regions of normal tissue.

Discussion

In this study, a visual comparison was initially performed between histology and OCT images of biopsy specimens obtained from solid and oral mucosal lesions. In Fig. 2c, d, the OCT image intensity is seen to decrease as a function of depth into the tissue. This phenomenon is governed by OCT optics and light scattering within the tissue. The inherent ambiguity in the source of decreasing image brightness is somewhat mitigated in SID because it relies upon relative changes measured by the same OCT instrument. However, this is an unsatisfactory situation for wider clinical adoption and result comparison. This has resulted in a recent surge of activity to develop standards and calibration phantoms for OCT [18, 20].

Furthermore, Fig. 2 highlights an additional difficulty with the direct comparison of OCT and histology images due to various sources of geometric distortion. Such effects are well-known in histopathology. OCT is similarly affected by sample rotation, refractive index and instrument optics. The difficulty with identification of identical tissue sections in both modalities is a further complication. These factors compound to result in imperfect visual correlation between OCT and histology. One of the advantages of SID is that it augments the OCT B-scan view by providing an overview of an area of tissue.

In OCT, the fluid-filled lesions are characterised by a discontinuous drop in the intensity of backscattered light at the tissue–fluid interface. Typically, the fluid-filled region exhibited little or no backscattered signal compared to surrounding cellular structures due to the lack of optical scattering centres. This sharp signal intensity drop is apparent in Fig. 2d below the epithelium and contrasts with the continuous gradual decay in the optical signal strength as a function of depth observed in normal tissue (Fig. 2c). This optical phenomenon is confirmed by a similar profile of stain uptake in histology. Whilst morphological analysis is the gold standard for diagnosis, histological stain uptake facilitates the interpretation of OCT signal intensities which originate from light scattering within the tissue. This approach is well established for quantitative assessment of OCT data from tissue [5, 21].

For this work, $n \approx 10^6$ independent SID measurements were obtained per sample. This provided a high level of confidence in the statistical distributions of SID values that were identified as approximately normal (Fig. 3a). Under these conditions, the t test model was appropriate and confirmed the fluid-filled and control groups to be significantly different. Therefore, these results represent >95 % confidence that SID can provide a measurable difference between fluid-filled and solid lesions. Furthermore, the point SID measurements were found to discriminate between fluid-filled and solid tissue with a sensitivity and specificity of

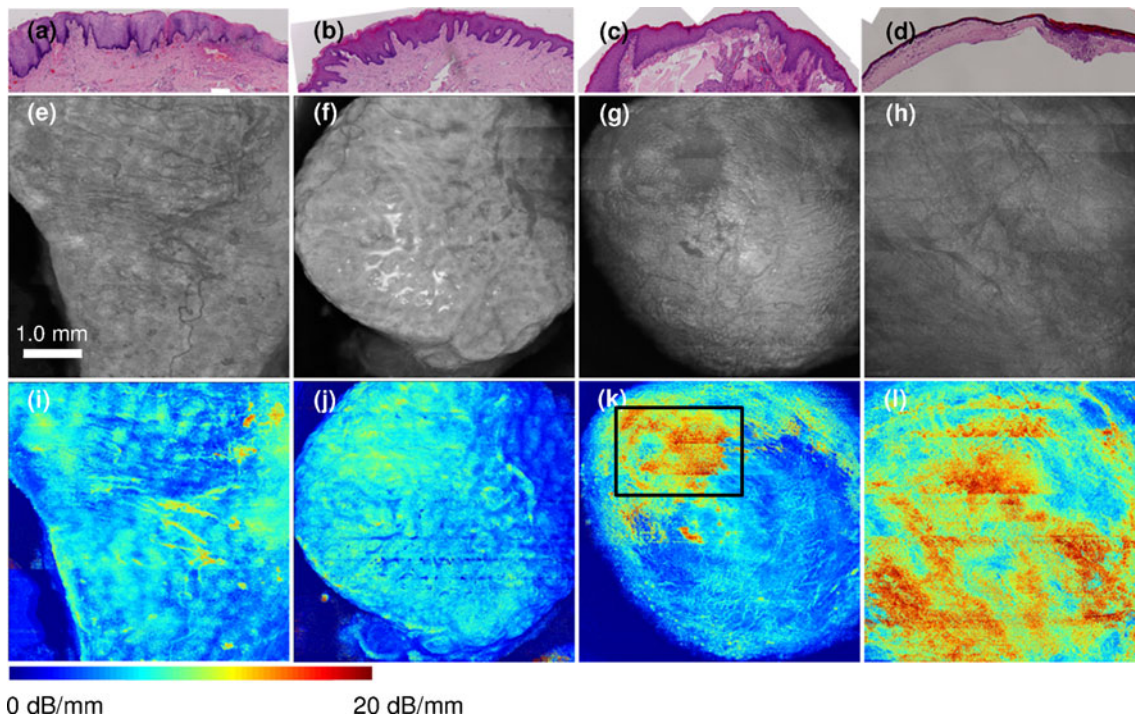


Fig. 4 Histology sections (**a–d**) from which diagnosis was established by the pathologist. Corresponding intensity images (**e–h**), where each pixel is calculated from the sum of each OCT A-scan. SID images of the same tissue samples (**i–l**), where each pixel is calculated using the SID analysis procedure. Examples are of two normal control biopsy

samples (**a, b, e, f, i, j**) and two specimens containing fluid-filled regions (**c, d, g, h, k, l**) visualised in the SID images of regions of intense red colouration. The *colour bar* represents SID values in the range 0–20 dB/mm

80 % (Fig. 3b). However, the intended purpose for these SID values is to generate images rather than as single point diagnostic measurements. Thus, visual inspection of SID images confirms that high SID regions exist within the fluid-filled areas of tissue. This provides additional support to the statistical findings.

The averaged OCT depth profiles (insets in Fig. 2c, d) do not reflect the spatial variation in tissue architecture because they contain contributions from across the sample, referenced to the surface. In a similar manner, individual cross-sectional images are not necessarily representative of an entire biopsy sample or large areas of oral mucosa. Furthermore, direct visual assessment of three-dimensional OCT datasets of large tissue volumes can be challenging. These limitations therefore necessitate a compression of the dataset such that it can be readily visualised clinically. To accomplish this, spatial variation of the SID parameter over an entire tissue volume was mapped on to a false colour en face (surface) image as shown in Fig. 4i–l. These images show regions of high SID in fluid-filled areas, thus augmenting the underlying 3D morphological OCT data. However, some horizontal banding is present. This is due to the data acquisition protocol imposed by the OCT instrument used for this study. Hence, tissue volumes measuring several millimetres were acquired in batches of 100 B-scans.

Inevitably, sample movement of approximately 10–100 μm between successive segments led to the visible discontinuities. In this study, mucoceles were used as a representative model for rare oral lesions that may contain fluid within or below the epithelium. This was justified on the basis that the mucinous fluid in mucoceles and inflammatory exudates in blistering lesions are both largely acellular. Consequently, they both demonstrated low optical backscattering [22, 23].

Comparison between subpanels c and k of Fig. 4 demonstrates the ability of SID imaging to identify a localised region of fluid collection. In addition, Fig. 4k also displays peri-lesional areas which can be important for selecting the most representative biopsy site in blistering diseases of the oral mucosa. It has been previously reported that this is a critical factor in determining the sensitivity of direct immunofluorescence, a crucial diagnostic tool for immune diseases of the oral mucosa [24]. Figure 4l demonstrates an extensive area of fluid collection imaged using SID and confirmed by histology (Fig. 4d). Figure 4k and l is indicative of SID's capability to visualise lesional extent in vivo. Disease extent is implicated as a key parameter for grading the severity of oral blistering lesions [25].

Intra-orally, OCT complemented by SID analysis would facilitate non-invasive objective visualisation of the entire oral mucosa for fluid-filled areas. This would enable

sampling of multiple lesions from individual patients. Moreover, SID would permit monitoring of the therapeutic effects of medication used in the management of blistering oral lesions, such as mucous membrane pemphigoid and pemphigus.

This quantitative approach provides a specific contrast mechanism for fluid-filled lesions. Whilst this study was performed on *in vitro* tissue samples, it represents significant potential advantages over conventional visual inspection. One of the most important attributes is that it can reveal the extent of a fluid-filled area beyond that which can be observed by the naked eye alone. Consequently, tissue that would normally not be considered for biopsy selection may be selected, thus providing pathologists with representative samples on which to make a definitive diagnosis. Although this study was confined to the oral cavity, SID is applicable to other mucosal surfaces and hence may be useful in multiple clinical specialities.

Acknowledgments The authors acknowledge the financial support of the Institute of Dentistry, Queen Mary, University of London. The EX1301 OCT microscope used in this study was on loan from Michelson Diagnostics Ltd. We also thank Professor Kim Piper for providing the histopathology reports.

Conflict of interest The authors declare no conflict of interest.

References

1. Wilder-Smith P, Hammer-Wilson MJ, Zhang J, Wang Q, Osann K, Chen Z, Wigdor H, Schwartz J, Epstein J (2007) *In vivo* imaging of oral mucositis in an animal model using optical coherence tomography and optical Doppler tomography. *Clin Cancer Res* 13:2449–2454
2. Fujimoto JG, Bouma B, Tearney GJ, Boppart SA, Pitris C, Southern JF, Brezinski ME (1998) New technology for high-speed and high-resolution optical coherence tomography. *Ann N Y Acad Sci* 838:95–107
3. Huang D, Swanson EA, Lin CP, Schuman JS, Stinson WG, Chang W, Hee MR, Flotte T, Gregory K, Puliafito CA et al (1991) Optical coherence tomography. *Science* 254:1178–1181
4. Armstrong WB, Ridgway JM, Vokes DE, Guo S, Perez J, Jackson RP, Gu M, Su J, Crumley RL, Shibuya TY, Mahmood U, Chen Z, Wong BJ (2006) Optical coherence tomography of laryngeal cancer. *Laryngoscope* 116:1107–1113
5. Tsai MT, Lee CK, Lee HC, Chen HM, Chiang CP, Wang YM, Yang CC (2009) Differentiating oral lesions in different carcinogenesis stages with optical coherence tomography. *J Biomed Opt* 14:044028
6. Ozawa N, Sumi Y, Chong C, Kurabayashi T (2009) Evaluation of oral vascular anomalies using optical coherence tomography. *Br J Oral Maxillofac Surg* 47:622–626
7. Lee CK, Tsai MT, Lee HC, Chen HM, Chiang CP, Wang YM, Yang CC (2009) Diagnosis of oral submucous fibrosis with optical coherence tomography. *J Biomed Opt* 14:054008
8. Adegun OK, Tomlins PH, Hagi-Pavli E, McKenzie G, Piper K, Bader DL, Fortune F (2011) Quantitative analysis of optical coherence tomography and histopathology images of normal and dysplastic oral mucosal tissues. *Lasers Med Sci* 27:795–804
9. Bazant-Hegemark F, Stone N (2008) Near real-time classification of optical coherence tomography data using principal components fed linear discriminant analysis. *J Biomed Opt* 13:034002
10. McLaughlin RA, Scolaro L, Robbins P, Saunders C, Jacques SL, Sampson DD (2009) Mapping tissue optical attenuation to identify cancer using optical coherence tomography. *Med Image Comput Assist Interv* 12:657–664
11. Tomlins PH, Adegun O, Hagi-Pavli E, Piper K, Bader D, Fortune F (2010) Scattering attenuation microscopy of oral epithelial dysplasia. *J Biomed Opt* 15:066003
12. Levitz D, Thrane L, Frosz M, Andersen P, Andersen C, Andersson-Engels S, Valanciunaite J, Swartling J, Hansen P (2004) Determination of optical scattering properties of highly-scattering media in optical coherence tomography images. *Opt Express* 12:249–259
13. Barwari K, de Bruin DM, Cauberg ECC, Faber DJ, van Leeuwen TJ, Wijkstra H, de la Rosette J, Laguna MP (2011) *J Endourol* 25:311–315
14. Cauberg ECC, de Bruin DM, Faber DJ, de Reijke TM, Visser MV, de LA Rosette JJMCH, van Leeuwen TG (2010) Quantitative measurement of attenuation coefficients of bladder biopsies using optical coherence tomography for grading urothelial carcinoma of the bladder. *J Biomed Opt* 15:066013
15. Soest VG, Goderie TPM, Regar E (2010) Atherosclerotic tissue characterization *in vivo* by optical coherence tomography attenuation imaging. *J Biomed Opt* 15:011105
16. Scolaro L, McLaughlin RA, Klyen BR, Wood BA, Robbins PD, Saunders CM, Jacques SL, Sampson DD (2012) Parametric imaging of the local attenuation coefficient in human axillary lymph nodes assessed using optical coherence tomography. *Biomed Opt Express* 3:366–379
17. Tomlins PH, Ferguson RA, Hart C, Woolliams P (2009) Point spread function phantoms for optical coherence tomography. National Physical Laboratory, Report OP2, ISSN 1754-2944. <http://www.npl.co.uk/publications/point-spread-function-phantoms-for-optical-coherence-tomography>
18. Woolliams PD, Tomlins PH (2011) The modulation transfer function of an optical coherence tomography imaging system in turbid media. *Phys Med Biol* 56:2855–2871
19. Thrane L, Yura HT, Andersen PE (2000) Analysis of optical coherence tomography systems based on the extended Huygens-Fresnel principle. *J Opt Soc Am A* 17:484–490
20. Woolliams PD, Ferguson RA, Hart C, Grimwood A, Tomlins PH (2010) Spatially deconvolved optical coherence tomography. *Appl Opt* 49:2014–2021
21. Tsai MT, Lee HC, Lee CK, Yu CH, Chen HM, Chiang CP, Chang CC, Wang YM, Yang CC (2008) Effective indicators for diagnosis of oral cancer using optical coherence tomography. *Opt Express* 16:15847–15862
22. Angelova-Fischer I, Pfeuti T, Zillikens D, Rose C (2009) *In vivo* confocal laser scanning microscopy for non-invasive diagnosis of pemphigus foliaceus. *Skin Res Technol* 15:40–44
23. Levi A, Ophir I, Lemster N, Maly A, Ruzicka T, Ingber A, Enk CD (2011) Noninvasive visualization of intraepidermal and subepidermal blisters in vesiculobullous skin disorders by *in vivo* reflectance confocal microscopy. *Lasers Med Sci* 27:261–266
24. Sano SM, Quarracino MC, Aguas SC, Gonzalez EJ, Harada L, Krupitzki H, Mordoh A (2008) Sensitivity of direct immunofluorescence in oral diseases. Study of 125 cases. *Med Oral Patol Oral Cir Bucal* 13:E287–E291
25. Mignogna MD, Fortuna G, Leuci S, Adamo D, Dell'aversana Orabona G, Ruoppo E (2010) Adjuvant triamcinolone acetonide injections in oro-pharyngeal pemphigus vulgaris. *J Eur Acad Dermatol Venereol* 24:1157–1165